http://dx.doi.org/10.1016/j.apenergy.2023.122422

Evaluation of various collector configurations for a photovoltaic thermal system to achieve maximum performance, low cost and light weight

Arash Kazemian[1,2], Tao Ma[2*], Yang Hongxing[1*]

[1]*Department of Building Environment and Energy Engineering, The Hong Kong Polytechnic University, Hung Hom, Kowloon, Hong Kong*

[2]*School of Mechanical Engineering, Shanghai Jiao Tong University, Shanghai, China*

*Corresponding authors: tao.ma@sjtu.edu.cn (T. Ma); hong-xing.yang@polyu.edu.hk (H. Yang)

Abstract

This study evaluates different collector configurations of a photovoltaic thermal system to identify the most effective design for achieving high electrical and thermal powers, exergy, low-pressure drops, and short payback time. Based on the authors' most recent information, previous studies have identified three gaps in the literature: rare research on the comparison between various collector designs such as grids, serpentine paths, wavy paths, parallel paths, spiral paths, etc.; little research on the distribution of surface temperature and pressure drop for different collector configurations under the same wetted area; and a lack of consideration of the cost and weight of collector and absorber layers for different materials. To address these research gaps, we investigated various collector designs, lengths and materials and analyzed their impact on the system performance. Our findings demonstrate that the photovoltaic thermal system with the multipath serpentine design is the most effective in terms of overall power, with an average overall power output of 423.84 W/m^2. Furthermore, the photovoltaic thermal system with aluminum offers the most significant cost efficiency, with a payback time of 2.58 years, and weighs 42% less than the system with copper.

Keywords:

Photovoltaic thermal; Collector design; Energy and exergy analysis; Economic analysis; System weight and pressure drop

Nomenclature	
A	Area (m^2)
C_e	Electricity price (US \$.kWh^{-1})
C_{ng}	Natural gas price (US \$.kWh^{-1})
C_0	Investment cost (US \$)
$C_{O\&M}$	Operation and maintenance (O&M) costs (US \$)
c_P	Specific heat capacity ($J.kg^{-1}.K^{-1}$)
CS_{S-CCHP}	Annual cost savings (US \$)
d	Discount rate
E	Energy (J)
E''	Rate of energy ($W.m^{-2}$)
Ex''	Rate of exergy ($W.m^{-2}$)
E_{Cov}	Annual produced electrical power (kWh)
h	Convection heat transfer coefficient ($W.m^{-2}.K^{-1}$)
i_F	Fuel inflation rate
k	Thermal conductivity coefficient ($W.m^{-1}.K^{-1}$)
$\dot{m}$	Mass flow rate ($kg.s^{-1}$)
P	Pressure (Pa)
t	Time (s)
T	Temperature (K)
V	Velocity ($m.s^{-1}$)

Greeks

α	Absorptivity
β	Reference temperature coefficient
ε	Emissivity
η_r	Energy efficiency reference (%)
η_{boil}	Energy efficiency of boiler (%)
μ	Dynamic viscosity ($kg.m^{-1}.s^{-1}$)
ρ	Density ($kg.m^{-3}$)
σ	Stefan-Boltzmann constant ($W.m^{-2}.K^{-4}$)
τ	Transmissivity
ω	Dust deposition ($g.m^{-2}$)

Subscripts

ab	Absorber
amb	Ambient
eff	Effective
el	Electrical
g	Glass cover
HTF	Heat transfer fluid
pv	Photovoltaic unit
ref	Reference
s	Solid components
th	Thermal
w	Wind

Abbreviation

PBT	Payback time
PV	Photovoltaic unit

1 Introduction

The development of alternative energy technologies has been increasing in response to the growing energy demand and environmental concerns associated with fossil fuel usage. The accessibility and affordability of solar energy make it a highly attractive energy source. Photovoltaic (PV) units can convert solar irradiation into heat and electricity. Currently available PV modules convert 9-20% of sunlight into electricity [1], whereas the rest of 80-91% is absorbed or reflected. By absorbing large amounts of solar energy, the module's performance and lifespan can be reduced due to increased cell temperature [2]. Photovoltaic thermal (PVT) modules address this issue by combining solar PV units with solar thermal collectors, allowing for converting energy absorbed by cells into electricity and heat. While PVT systems have higher electrical and overall power than standalone PV units, further refinement is needed to make them more suitable. There has been considerable research on improving the performance of PVT systems, such as optimizing collector and absorber structures.

The design of a flow field in a photovoltaic-thermal (PVT) system is critical in achieving uniform, stable power output with low weight and cost. Three of the most common collector configurations for PVT systems are parallel, serpentine, and spiral flow fields [3]. Each design has its advantages and disadvantages, which are determined by factors such as the distribution of pressure drop, the maximum speed in collector tubes, and the surface of contact with the absorber plate that facilitates heat transfer. Additionally, the dimensions and material of the different configurations can be modified, influencing the final performance. The parallel flow tube is the simplest version, as it consists of a series of parallel flow tubes joined at the entrance and exit of the system. This design

has very low pressure drops as a result of the even division of the fluid through numerous parallel tubes with no directional shifts [4]. Conversely, the serpentine flow pattern has larger pressure drops between the inlet and outlet, as the water is forced to follow parallel and serpentine paths that take up the whole panel [5]. Finally, the spiral flow field has 90° turns rather than 180° turns in serpentine flow fields, resulting in a more uniform flow distribution [6]. Designing a flow field requires achieving maximum heat homogeneity over the PV cells' area and improving water management with minimal pumping power consumption. To this end, several attempts have been made to optimize the flow pattern arrangement in order to maximize PVT output.

Poredoš et al. [7] analyzed numerically and experimentally the study of three different channel geometries for a Photovoltaic Thermal (PVT) system: U-shape, parallel, and bionic. The bionic structure achieved the greatest electrical efficiency of 14.5% and the lowest pressure drop of 385 Pa. Fudholi et al. [8] compared the web, parallel, and spiral collector designs of a PVT system under the constant intensity of 800 W/m2 and a flow rate of 0.04 kg/s. The spiral design achieved the highest electrical and thermal performance, with 13.8% and 54.6%. Palaskar and Deshmukh [9] compared the U-shaped, parallel, and split flow configurations of a PVT module through a steady numerical simulation under a variety of solar radiations. The split flow design achieved the highest thermal efficiency, while the U-shaped design had the lowest thermal efficiency. Finally, Hossain et al. [10] analyzed a PVT system with a two-sided serpentine collector design, reporting thermal energy efficiency and overall exergy efficiency of 87.72% and 11.08%, respectively. A PVT system with wavy collectors was simulated by Eisapour and al. [11]. Various amplitudes of wavy tubes and straight parallel tubes were considered. They found that PVT systems with parallel tubes had electrical and thermal energy efficiency of 10.94% and 61.04%. The outputs for the system with wavy tubes are 11.32% and 65.21%, respectively. Shahsavar [12] examined PVT

systems with wavy serpentine tubes and plain serpentine tubes in another study. Using magnetite nanofluid as a coolant, they investigated the effects of parameters like the wavy collectors' wavelength and amplitude. According to the study, the wavy serpentine tube system was more energy efficient for electrical and thermal energy than the plain serpentine tube system by 20.67-30.63% and 1.94-2.32%, respectively.

Aside from the mentioned standard designs, there have been many variations, such as adding curved corners [13], inserting inserts inside tubes [14], or changing parameters, for instance, the tube number [15], the tube diameter [16], or the cross-sectional shape [17], adding thermal storage mechanisms [18], adding fin-faom designs [19], and using triplex-tubes [20]. The designs are all intended to be easy to manufacture while meeting the four general performance requirements (uniform PVT surface temperature distribution, high thermal and electrical power, low pressure drop) [21]. The selection of an efficient material for the collector and absorber is just as important as the design of the collector geometry. Factors such as thermal conductivity, ease of handling, cost, and weight should all be taken into account when selecting the material. Copper, aluminum, and steel are commonly used for PVT systems' collector tubes and absorber plates. Aluminium has a relatively high thermal conductivity and is light in weight, but copper is heavier and more expensive. Steel is cheap, but it is also heavy and has low thermal conductivity. The lightweight feature of the PVT system is particularly important in conditions where weight is a critical factor, such as in portable or mobile applications where the weight of the PVT system affects its portability or maneuverability. Additionally, in applications where the PVT system is mounted on rooftops or other structures, the weight of the system can affect the structural integrity of the building. To evaluate the prospect of the lightweight feature, it is essential to analyze the weight of the PVT system with different materials for the collector and absorber layers, as well as different

collector lengths. The ideal collector material should have high transfer capabilities, low weight, and low cost. Additionally, the design should minimize material consumption. Therefore, assessing the functionality of PVT systems with various collector materials and lengths is significant.

Based on the authors' most recent information, previous studies have identified three gaps in the literature: (a) rare research on the comparison between various collector designs such as grids, serpentine paths, wavy paths, parallel paths, spiral paths, etc.; (b) little research on the distribution of surface temperature and pressure drop for different collector configurations under the same wetted area; and (c) a lack of consideration of the cost and weight of collector and absorber layers for different materials.

In light of these gaps, the following research objectives and aims are proposed:

- To compare different PVT system collector configurations, namely parallel, spiral, serpentine, wavy, grid, multipath design, split flow, etc.
- To study how collector design impacts energy, exergy, and pressure drop in PVT systems under transient weather conditions.
- To examine the influence of multiple variables on system capability, pressure drop, and weight, such as collector wetted area and collector tubes and absorber layer material.
- To evaluate the costs and determine the payback time of PVT with diverse materials consisting of copper, aluminum, stainless steel, and brass for collector tubes and absorber layers.

The proposed theory and technology can be applied to the engineering of photovoltaic thermal (PVT) systems in various ways, such as optimizing collector design, material selection, and

pressure drop analysis. Engineers can use the proposed theory and technology to analyze the impact of different design parameters, such as the collector shape, tube diameter, and length, on energy and exergy efficiencies, pressure drop, and cost, leading to better design and optimization outcomes. Additionally, the proposed technology can evaluate the impact of different materials for the collector and absorber layers on the cost and weight of PVT systems, enabling engineers to determine which material offers the best balance of performance, cost, and weight.

Moreover, the proposed theory and technology can be used to analyze the pressure drop in PVT systems and identify ways to reduce it, leading to improved system performance and efficiency. Overall, the proposed theory and technology offer a powerful tool for improving the design and performance of PVT systems, resulting in significant improvements in the efficiency and accuracy of PVT system modeling and analysis.

2 Methodology

Fig 1 outlines the method used in this work to assess comparisons between various collector designs of a PVT device on energy and exergy output, cost-effectiveness, pressure drop, and weight. The high performance of a PVT system can be achieved through suitable design and material selection. In our study, the system performance iss assessed by selecting suitable collector design, material, and collector length. Thus, first, numerical models are developed for various systems under consideration. The accuracy of these models has been verified by comparing them to experimental and numerical results reported in the literature. A comparison is carried out to examine the consequences of collector design on system performance at a constant collector total length (see Section 3.1).

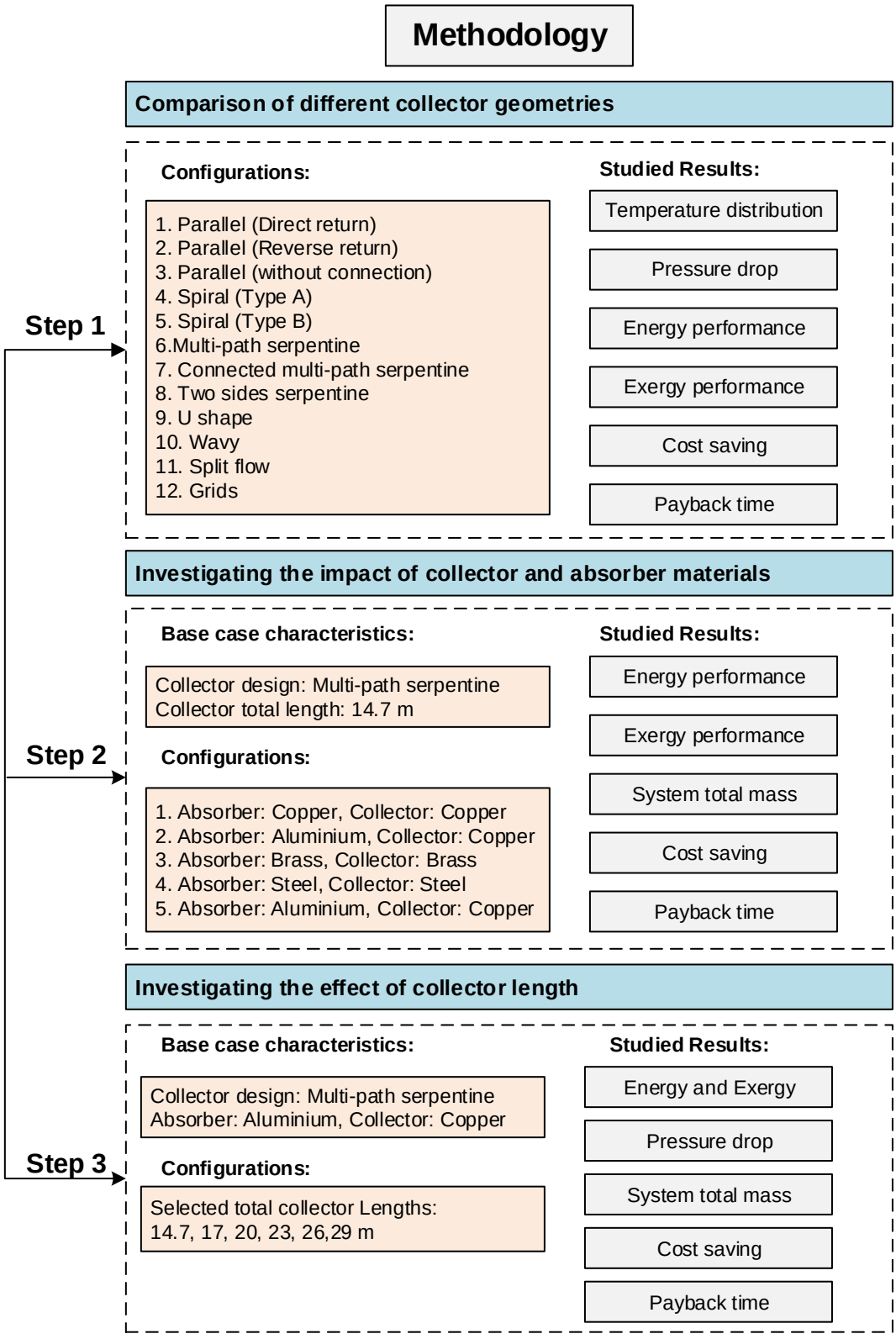

Fig 1. The methodology flowchart of the research study.

Furthermore, the effects of the material used for the collector and absorber on the system's total weight, cost, and performance are investigated in Section 3.2. In this section we have selected Multi-surpentine path as collector design with total collector tube length of 14.7 m.

Lastly, the impact of altering the total length of the collector tubes in a base-case PVT system with a multipath serpentine design featuring an aluminum absorber and copper collector is examined in Section 3.3.

2.1 Designs description

This study numerically simulates the PVT system in 3D with various collector configurations. Cases are selected based on common types of designs used in the literature. Moreover, some novel designs are also employed to find the most suitable design. Parallel designs are one of the traditional types which are used in previous research. Researchers used different types of parallel configurations in their systems. The first type of parallel design is illustrated in Fig 2-(a), which is called parallel (direct return). In this design, the length of the water circuit through the inlet and outlet piping to each parallel tube is different, and tubes near the outlet have a larger flow rate. Another type of parallel design is presented in Fig 2-(b), which is called parallel (Reverse return). In contrast, in the reverse return system, presented in Fig 2-(b), supply and return are the same lengths throughout the collector, making it possible that all parallel tubes have nearly the same flow rate. Another parallel design that is mostly used in research is presented in Fig 2-(c), consisting of several parallel tubes, and there is no connection between them; all tubes have the same flow rate. Two different spiral collector designs are also investigated, and their difference is in the position of the outlet, as seen in Fig 2-(d) and (e). Serpentine design is also another configuration that is used in PVT systems. The most common serpentine collector design is a simple serpentine collector, which appears in Fig 2-(i). Additionally, three other serpentine

configurations (Fig 2-(f), (g), and (h)) are also investigated, and only a few studies are available about them in the literature.

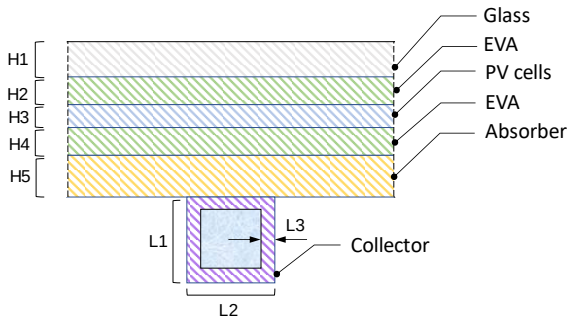

(m) Cross section of PV layers, absorber and collector

Fig 2. Various collector configurations of PVT system [7, 22, 23]

Wavy, split flow, and grid designs are also evaluated, shown in Fig 2-(j)-(l). All proposed systems in Fig 2 include PV cells, a glass cover that covers the PV cells, an absorber at the bottom of the PV cells, and collector tubes beneath the absorber. Apart from the PV surface, the PVT system is fully insulated [24]. In cases with multiple entrances, namely parallel design (without connection) and multipath serpentine, it is presumed that the mass flow rate is split evenly between entries. All cases are evaluated using the same total length of collector, tube diameter, and PV layers to evaluate the effect of the collector design illustrated in Fig 2-(m). When we refer to the total length of the collector tube, we mean the entire length of the collector tubes that are used in the system (The component which is presented by purple color in Fig 2.

Table 1. Geometric parameters of selected configurations are presented in Fig 2 (It should be noted that for all cases in Fig 2, X1=2000, X2=1000, H_1=3.5, H_2=0.5, H_3=0.3, H_4=0.5, H_5=1.5, L_1=17, L_2=17, L_3=1 mm and the total length of collectors are same.)

Cases	Dimensions (mm)
Parallel (Direct return)	A=124.14, B=1665, C=90.45
Parallel (Reverse return)	A=124.14, B=1665, C=90.45
Parallel (without connection)	A=132, B=1839
Spiral (Type A)	A= 110.74, B= 440.78, C= 438.78, D= 164.90
Spiral (Type B)	A=76.26, B=107.82, C=165.84, D=253.03, E=270.03
Multipath serpentine	A= 132.50, B= 132.50, C= 1654.50
Connected multipath serpentine	A= 62.50, B= 143.66, C= 800.13
Two sides serpentine	A= 104, B= 254, C= 135.5, D=239
Wavy	A=135, B=132.4, C=210.03, D=64.65, E= 132.46, F=92.46, G= 1724.62
Split flow	A=88.95, B=175, C=138.81, D=158, E=610.11, F=288.93
Grids	A=297, B= 249.40, C=61.5

Utilizing the same wetted area for comparison of the effect of different collector designs of PVT systems has more accuracy because it eliminates any potential differences in the amount of heat transfer that differences in the surface area of the collectors could cause. This ensures that any differences in performance are due to the design of the collector rather than any differences in the amount of heat transfer. Additionally, different collector designs can be compared more accurately this way. The coolant which passes through the collector is water. Table 1 and Table 2 show various components' dimensions and thermophysical characteristics.

Table 2. Variations in elements' thermophysical characteristics [25, 26].

Components	Density ($kg.m^{-3}$)	Conductivity ($W.m^{-1}.K^{-1}$)	Specific heat ($J.kg^{-1}.K^{-1}$)
Glass	2200	0.76	830
EVA	960	0.35	2090
PV cells	2330	148.0	700
Copper	8978	387.6	381
Aluminium	2719	202.4	871

Brass	8390	123	380
Stainless steel	8030	16.27	502.48

2.2 Numerical solution

In this study, the 3D PVT cases in this project are simulated using SolidWorks and numerically modeled using ANSYS Fluent 18.2. Assuming incompressible low-speed flow, numerical calculations are carried out using a pressure-based approach. As the Reynolds number is low, laminar conditions are taken into account for the fluid regime. Also, the SIMPLE algorithm couples pressure and velocity components [27]. Discrete convection terms are obtained using the second-order upwind approach [28, 29]. A transient model with a time step of 600s is considered. The sum of residuals of the continuity, momentum, and energy functions are deemed convergence for residuals below $10^{-5,}$ 10^{-5}, and 10^{-7}, respectively.

2.2.1 Main assumptions and hypothesis

The following are the assumptions that were considered for numerical modeling:

- Assimilation of the sky as a black body [13]: The sky is treated as a surface that absorbs all radiation incident upon it and emits radiation according to its temperature, simplifying the calculation of the radiative heat transfer between the sky and the collector.
- A PVT collector is considered to have a uniform ambient temperature around it [30]: The temperature around the PVT collector is assumed to be uniform, and does not vary significantly with location, simplifying the calculation of convective heat transfer between the collector and the surrounding air.
- The PV/T module's sidewalls and bottom are ideal insulators, and minimal heat transfer to the environment occurs [31]: The PV/T module is assumed to be perfectly insulated on its

sides and bottom, and that very little heat is transferred to the environment through these surfaces, simplifying the focus on the heat transfer processes occurring within the PV/T module itself.

- PVT surface is not coated with dust or agents [32]: The PVT surface is assumed to be perfectly clean, without any dust or other agents that could affect its absorption and reflection of solar radiation, isolating the effects of other factors on the performance of the PVT collector.
- Transmission of 100% is presumed for the EVA layer [13, 33]: The EVA layer, which is used to encapsulate the PV cells, is assumed to have a perfect transmission rate for solar radiation, allowing all incident radiation to pass through to the PV cells and focusing on the performance of the PV cells themselves.
- Absorbed solar radiation is considered as an energy source in PV cells [34]: The absorbed solar radiation is considered as the primary energy source for the PV cells, and is used to generate electrical power, which is fundamental to the operation of PV cells.
- Working fluids and solid components have temperature-independent thermophysical properties [31]: Since temperature variation in system is not so high, the thermal properties of the working fluids and solid components used in the model, such as thermal conductivity and specific heat, are assumed to be independent of temperature, simplifying the calculation of heat transfer and fluid flow processes in simulations.
- Each entrance receives an equal amount of coolant mass flow in cases that have more than one entrance, such as parallel (without connection) and multipath serpentine as shown in Fig 2-(c) and (f). Thus, the multipath serpentine design with two entrances has a mass flow

rate of $\dot{m}/2$ at each entrance, while the parallel (without connections) design has a mass flow rate of $\dot{m}/8$ since there are eight entrances.

2.2.2 Governing equations

Based on the assumptions above, the governing equations are explained below. Solid parts transfer heat by conduction, and the corresponding equation is presented as follows [35]:

$$(\rho c_p)_s \frac{\partial T_s}{\partial t} = \nabla \cdot \left(k \nabla T\right)_s + \gamma \left(E''_{eff,sun} - E''_{el}\right) \quad (1)$$

where density, specific heat capacity, and thermal conductivity are represented by ρ, c_p and k, respectively. The letter s in subscript form is used to denote solid components.

User-defined functions (UDFs) are utilized in this equation to generate two source terms of effective solar power absorbed by PV ($E''_{eff,sun}$) and the electricity generated by PV (E''_{el}). PV cells therefore have $\gamma = 1$, while other solid components have $\gamma = 0$. Calculating two source terms is described below [36]:

$$E''_{eff,sun} = \tau_g \alpha_{pv} G_{sun} A_{pv} \quad (2)$$

$$E''_{el} = E''_{eff,sun} \cdot \eta_r \cdot \left[1 - \beta \cdot \left(T_{cell} - T_{ref}\right)\right] \quad (3)$$

Eq (2) includes glass transmissivity ($\tau_g = 0.95$), PV absorptivity ($\alpha_{pv} = 0.90$) and area ($A_{pv} = 2\ m^2$). Eq.(3) provides a simplified model for calculating the electricity output of a PV panel that takes into account the temperature dependence of the panel's power output. The equation is based on several assumptions, including the assumption that the PV panel's efficiency, η_r, is constant and the irradiance or solar radiation received by the PV panel, $E''_{eff,sun}$, as a key parameter

influencing the power output. The temperature coefficient, β, is a measure of the decrease in the power output of the PV panel as the temperature of the panel's surface (T_{cell}) increases. This coefficient is typically given by the PV panel's manufacturer. The reference temperature, T_{ref}, is the temperature at which the temperature coefficient is measured. The equation assumes that the absorbed solar radiation is the primary energy source for the PV panel, and is used to generate electrical power. The equation can be used to estimate the electrical output of a PV panel based on the temperature of the panel's surface and the irradiance or solar radiation received by the panel. The equation provides a simplified model for calculating the electrical output of a PV panel and is widely used in studies of solar energy systems. In Eq (3), $\eta_r = 0.17$, $\beta = 0.0045$ and $T_{ref} = 298.15\,K$ refer to reference PV cells' efficiency and reference temperature [37]. T_{cell} in Eq (3) is the average temperature of PV cells obtained from Eq (1). Required equations for analyzing convection and conduction through the working fluid [38]:

$$\frac{\partial \rho_f}{\partial t} + \nabla \cdot (\rho V)_f = 0 \tag{4}$$

$$\rho_f \left[\frac{\partial V_f}{\partial t} + (V_f \cdot \nabla) V_f\right] = -\nabla \mathrm{P} + \nabla \cdot (\mu \nabla V)_f \tag{5}$$

$$(\rho C_p)\frac{\partial T_f}{\partial t} + (\rho C_p V \cdot \nabla T)_f = \nabla \cdot (k \nabla T)_f \tag{6}$$

where, the subscript of f denotes fluid, and P, V, μ express pressure, velocity, and dynamic viscosity of the coolant.

2.2.3 Boundary conditions

Considering a Reynolds number less than 2300, it is assumed that the velocity at the entry of the collector is constant. The temperature of flow at the entrance is the same as the ambient

temperature. There is a gauge pressure of zero pascal at the outlet, which is referred to "pressure outlet" boundary condition. The total inlet mass flow rate ($\dot{m}$) is 0.02 kg/s. There are some cases with only one entrance and others with more than one, as shown in Fig 2. When there are multiple entrances, the total mass flow rate is evenly distributed between each entrance, such as parallel (without connection) and multipath serpentine configurations, as shown in Fig 2-(c) and (f). Thus, the multipath serpentine design with two entrances has a mass flow rate of $\dot{m}/2$ at each entrance, while the parallel (without connections) design has a mass flow rate of $\dot{m}/8$ since there are eight entrances. Other cases with only one entrance have a mass flow rate of $\dot{m}$. The internal tube surfaces are subjected to a no-slip boundary condition. According to Eq.(1), solar radiation acts as an energy source. The side walls are kept adiabatic, except the top surface of the system (glass), which loses heat as convection and radiation mechanisms to the environment. This heat loss can be calculated using the convection heat transfer coefficient and sky temperature as follows [39]:

$$T_{sky} = 0.0552\, T_{amb}^{1.5} \tag{7}$$

$$h_{wind} = 5.7 + 3.8 V_w \tag{8}$$

Eq.(7) provides an estimate of the sky temperature as a function of the ambient temperature, assuming that the sky behaves as a blackbody with an emissivity of 1.0 and that it radiates energy to the ground and surrounding objects where T_{amb} and V_w are ambient temperature and wind velocity. Eq.(8) is a simplified model for estimating the convection heat transfer coefficient around a flat plate as a function of wind velocity when wind velocity is less than 5 m/s. In this equation, h represents the convection heat transfer coefficient in watts per square meter per degree Kelvin ($W/m^2 \cdot K$), and V represents the wind velocity in meters per second (m/s). This equation assumes the air temperature is equal to the ambient temperature. The equation is a simple linear function,

where the coefficient 5.7 represents the convection heat transfer coefficient in still air, and the coefficient 3.8 represents the increase in the heat transfer coefficient due to the presence of wind.

2.3 Performance evaluation

Four different performance parameters of the PVT system are compared, including power and exergy rate. Here are the thermal and electrical powers [40]:

$$E_{th}^{"} = \frac{m_f \times C_{p,f} \times (T_{f,out} - T_{f,in})}{A_{PV}} \tag{9}$$

$$E_{el}^{"} = E_{eff,sun}^{"} \cdot \eta_r \cdot \left[1 - 0.0045\left(T_{cell} - T_{ref}\right)\right] \tag{10}$$

Electrical exergy equals to electrical power [41], and thermal exergy can be determined by applying the following equations [42, 43]:

$$\dot{E}x_{th} = \dot{E}x_{mass,out} - \dot{E}x_{mass,in} = \dot{m}_f (\psi_{out} - \psi_{in}) \tag{11}$$

where [44]:

$$\psi_{out} = (h_{out} - h_{amb}) - T_{amb}(s_{out} - s_{amb}) \tag{12}$$

$$\psi_{in} = (\mathrm{h}_{in} - \mathrm{h}_{amb}) - T_{amb}(s_{in} - s_{amb}) \tag{13}$$

where s and h are the entropy values and specific enthalpy. By substitution of Eq.(12) and (13) in Eq.(11) and devided by area of the panel, the thermal exergy rate per unit area is calculated as follows [44]:

$$Ex_{th}^{"} = \frac{m_f \times C_{p,f} \left[\left(T_{f,out} - T_{f,in}\right) - T_{amb} \ln\left(\frac{T_{f,out}}{T_{f,in}}\right)\right]}{A_{pv}} \tag{14}$$

Solar systems are often evaluated using payback time (PBT) to determine when to recoup their investment costs. The PBT is calculated using the following equation [45]:

$$PBT = \frac{\ln\left[(C_0.(i_F - d))/(CS_{S-CCHP}) + 1\right]}{\ln\left[(1+i_F)/(1+d)\right]} \quad (15)$$

Assuming the fuel inflation rate to be 3.5% [45], where C_0 and i_F are the investment cost and the fuel inflation rate. Furthermore, a discount rate (d) of 5% is applied to the annual cost savings (CS_{S-CCHP}) [46]. Based on the assumption that electricity is not exported to the grid, the annual cost savings can be calculated as follows [45]:

$$CS_{S-CCHP} = E_{Cov} \cdot c_e + Q_{Cov} / \eta_{boil} \cdot c_{ng} - C_{O\&M} \quad (16)$$

where CS_{S-CCHP} is calculated utilizing the savings in electrical and natural fuel as a result of the solar system as well as the costs associated with operation and maintenance ($C_{O\&M}$). E_{Cov} and Q_{Cov} represent the annual electrical and thermal power, respectively, produced by a PVT system, with units of kWh. It is assumed that the system operates for six months of the year, from April to September. The electricity and natural gas prices per kWh (C_e and C_{ng}) in China are approximately 0.084 USD/kWh and 0.079 USD/kWh, respectively, as reported in reference [47]. Furthermore, the thermal power generated is supposed to be used instead of an 82% efficient gas-fired boiler (η_{boil}) [45]. Lastly, the $C_{O\&M}$ represents 1% of the total cost of a solar system [48].

2.4 Independence from the grid, as well as model confirmation

The ANSYS Workbench 18.2 software is used to create a 3D structure mesh with a refined grid near the collector walls, where there is a rapid change in temperature and velocity gradients. Water is employed as the operating fluid, and a multipath serpentine design is employed, with five distinct grid sizes created to enhance the precision and velocity of numerical modeling. The weather

conditions for the grid independence study are shown in Fig 4, and the flow rate equals 0.02 kg/s. Table 3 illustrates the coolant outlet's average temperature for various grid sizes.

The results indicate that the average outflow temperature is responsible for a 0.01 °C difference between 5.9 and 7.5 million mesh cases. Therefore, a grid of 5.9 million elements is selected for the remainder of the research, as a small discrepancy exists between simulations with 5.9 million and 7.5 million elements.

Table 3. Mesh independent study

Mesh (million)	Outlet temperature (ºC)	Difference from the case with 7.5 million meshes (ºC)
1.9	43.41	0.15
2.6	43.48	0.08
3.7	43.52	0.04
5.9	43.55	0.01
7.5	43.56	---

The outflow temperature of the PVT system was corroborated by employing numerical and experimental data from Khanjari et al.[49] and Selmi et al.[50]. Khanjari et al.[49] numerically simulated a PVT system and the model consisted of a glazing section, a PV panel, and a sheet-and-tube collector with five riser tubes, which were reduced to one to decrease computational effort. The model included an absorber plate and a water riser tube to consider heat transfer mechanisms. The geometry was created in CATIA software, and mesh generation and solution analysis were carried out in ANSYS Workbench. The fluid flow was assumed to be steady, incompressible, and uniform, and a fully developed laminar flow was taken for the simulation. The temperature distribution in the photovoltaic panel and absorber plate was assumed to be approximately the same. The amount of absorbed solar radiation was mainly related to the transmittance of glass, the absorbtance of the photovoltaic panel and absorber plate material, and

their effects were applied in the boundary conditions. Selmi et al.[50] conducted an experimental study to investigate the performance of a solar collector under different operating conditions. The solar collector was designed and built as a simple model consisting of a wooden box covered with transparent glass, containing an aluminum plate used as an absorber and a copper pipe for water flow. The housing frame was made of wood due to its high insulation efficiency and ease of forming. The model was 1.5 meters long, 166 millimeters wide, and 70 millimeters high, with an absorber plate and pipe fixed at a certain level inside the wooden box. The inner walls of the box, absorber plate, and pipe were covered by black mate paint, while the outside box was painted white. The pipe extended slightly on both sides outside the housing frame, in order to connect the water inlet and outlet fittings easily. A number of thermocouples were attached to the absorber plate, pipe at some selected points, and outside of the solar collector, to measure the collector inside, ambient, water inlet and outlet temperatures. The model was oriented to face the sun rays normally and tilted from time to time to keep tracing the sun position for most of the experiment time to gather maximum energy. These studies applied parallel design (without connection), 470-542 W/m^2 irradiance, 0.00136 kg/s flow rate, 32-46 ^oC inlet temperature, and water as the working fluid nearly identical in design and operation to the present work.

One difference between the current numerical model and the experiments performed by Selmi et al. [50] is that the PVT system in the current study is insulated, while Selmi et al. used a wooden box as insulation, which allowed for heat transfer to the environment. Additionally, Selmi et al. [50] considered tracing panels, while the current study assumed that the panel is fixed. The time span considered in the current study was from 7:00 to 17:00, while Selmi et al. [50] measured data from 9:30 to 13:15. Additionally, Khanjari et al. [49] made several key assumptions in their work, including assuming a steady-state condition and fully developed laminar flow. They also

approximated the temperature distribution in the photovoltaic panel and absorber plate to be approximately the same.

It should be noted that, for an accurate comparison, the same conditions were considered in the validation section, while the model and conditions related to this research were considered in the rest of the analysis. To determine the fluid temperature at the exit of the PVT system during the day, numerical and experimental techniques are compared with the present research, as seen in Fig 3. Results from the present study deviate from those of references [49] and [50] by an average of around 3% and 7%, respectively. The findings of this study show that the simulated PVT model is highly precise and dependable.

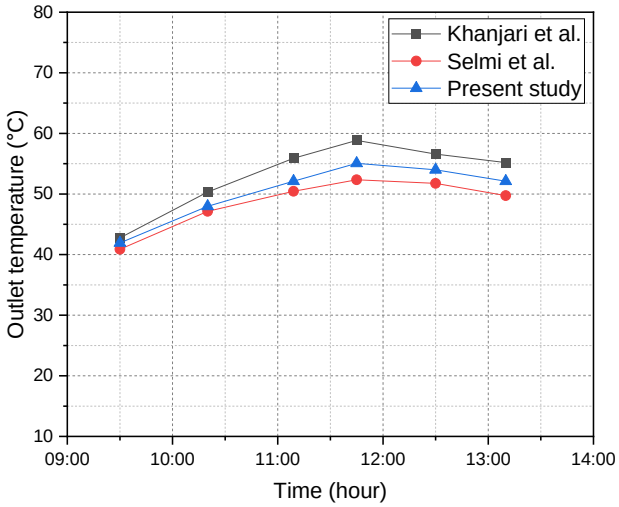

Fig 3. Validation of the outflow temperature obtained in the present work through numerical (Khanjari et al.[49]) and experimental (Selmi et al.[50]) studies

3 Results and discussion

The research was done in the summertime weather of Shanghai, China. Weather conditions considered in the simulation are displayed in Fig 4. The inflow temperature is assumed to vary with time and equals the ambient temperature. An open circuit system is used, in which water passes

through the collector only once before exiting. This type of system allows for the inlet of the collector to be directly connected to the city water, which is often stored in places that are in direct contact with the environment, such as dams. As a result, the temperature of the city water can change with the ambient temperature with a similar trend, and there is usually only a small difference between the two temperatures. This assumption is commonly used in several studies of PVT systems, and has been supported by other researchers in the field [13, 51]. The weather data used in our study was collected by the green energy laboratory of Shanghai Jiao Tong university. The profile shown in Fig 4 is based on the typical weather conditions during the summer season in Shanghai when the research was conducted. Specifically, the weather profile represents the average weather conditions during the summer period based on historical data for the region. Simulations were performed under transient conditions with a time step of 10 minutes. The corresponding weather conditions for each time step were used to calculate the electrical and thermal powers from 7:00 AM to 17:00 PM. An average value was then calculated. User-defined functions (UDFs) are used throughout the modeling process to consider all terms in Eq (1) and climate conditions. As a base case, dust deposition = 0 g/m^2, azimuth angle = 0°, tilt angle = 0°, wind speed= 1 m/s and total mass flow rate = 0.02 kg/s are used.

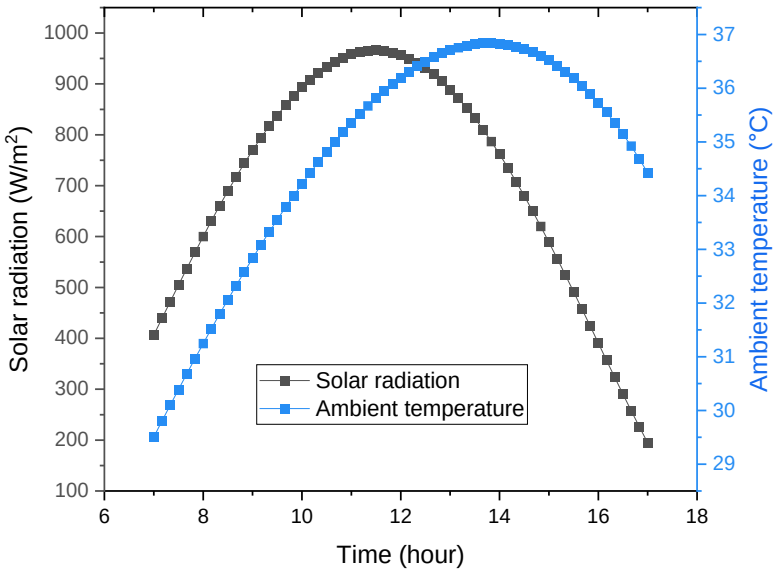

Fig 4. Typical July weather conditions in Shanghai.

3.1 Comparison of different collector geometries

A key parameter in determining a PVT system's performance is its absorber's temperature distribution. Different collector designs can have a significant impact on the temperature distribution of the absorber. In Fig 5, the contour of the temperature distribution of absorbers of PVT systems for different collector designs is compared. The same wetted area is used for this comparison to better evaluate the capability of different collector designs, and the simulation was based on a three-dimensional finite element model. In comparison to the temperatures near the collector's outlet, those close to the collector's inlet are cooler. This is due to the cooler water entering the collector than the water leaving it, resulting in a lower temperature near the inlet. Fig 5 also shows the highest surface temperature in parallel (direct return) collector design. This is because the length of the water circuit through the inlet and outlet piping to each parallel tube is different, resulting in tubes near the outlet having larger flow rates. The contours indicate that the

two-sided serpentine design has the lowest surface temperature, likely due to its large number of collector bends, facilitating a greater heat transfer.

Fig 5. The contour of the temperature distribution of the PVT systems absorber depends on the collector type.

Non-uniform temperature distribution is a common issue in PVT systems, and it can significantly impact the system's performance and efficiency. This non-uniformity can arise from various factors, such as variations in solar radiation intensity, shading, and non-uniform flow within the system. The uneven distribution of temperature can reduce the electrical and thermal efficiencies of the PVT system, which, in turn, can affect the module power generation. Hot spots and cold spots on the PV module due to non-uniform temperature distribution can lead to module degradation and reduced energy output. Based on Fig 5, it can be observed that the Spiral type A design has the most uniform temperature distribution and the lowest non-uniformity. In comparison, Case (a): Parallel (Direct return) has the highest non-uniformity. As a result, Spiral type A can generate nearly 1.6% higher electrical power than the Parallel (Direct return) design, as shown in Fig 6.

The results of Fig 6-(a) indicate that the multipath serpentine and parallel (without connection) designs are more effective in terms of thermal power than the other designs. The difference is owing to the total mass flow rate being equally divided between entrances, allowing for more efficient heat transfer. Furthermore, the temperature at each entrance is the same as the ambient temperature, increasing the temperature disparity from inlet to outlet, thus increasing the heat transfer rate.

Based on Fig 6-(b), the PVT system with a two-sided serpentine collector design has the greatest electrical power due to its low surface temperature, which allows almost half of the PV surface to remain at a low temperature during operation. The parallel (direct return) collector design has the lowest electrical power output due to its non-uniform flow rate in the parallel tubes. This is because the length of the water circuit through the inlet and outlet piping to each parallel tube is different, resulting in tubes near the outlet having larger flow rates. This means that the working fluid cannot absorb a large amount of heat, leading to a lower electrical power output.

The quality of thermal energy produced by the PVT system with different collector designs can be compared by examining the thermal exergy of the system as presented in Fig 6-(c). The findings suggest that the multipath serpentine and parallel (without connection) designs are more efficient regarding thermal exergy conversion than the other designs. This is since the thermal exergy of the systems is dependent on the inflow, outflow, and ambient temperature. Since inlet and ambient temperatures are equal in all cases, the systems with higher outflow temperatures have the maximum thermal exergy.

PVT systems are significantly affected by the pressure drop in the collector. Energy consumption increases as the pressure drop increases, resulting in an increase in pump power needed to maintain the flow rate. It can be observed in Fig 6-(d) that designs with more complex tube paths, such as two-sided serpentine collectors, have higher pressure drops (874 Pa), while designs with smoother tube paths, such as parallel tubes, split flow, and wavy, have lower pressure drops (less than 22 Pa).

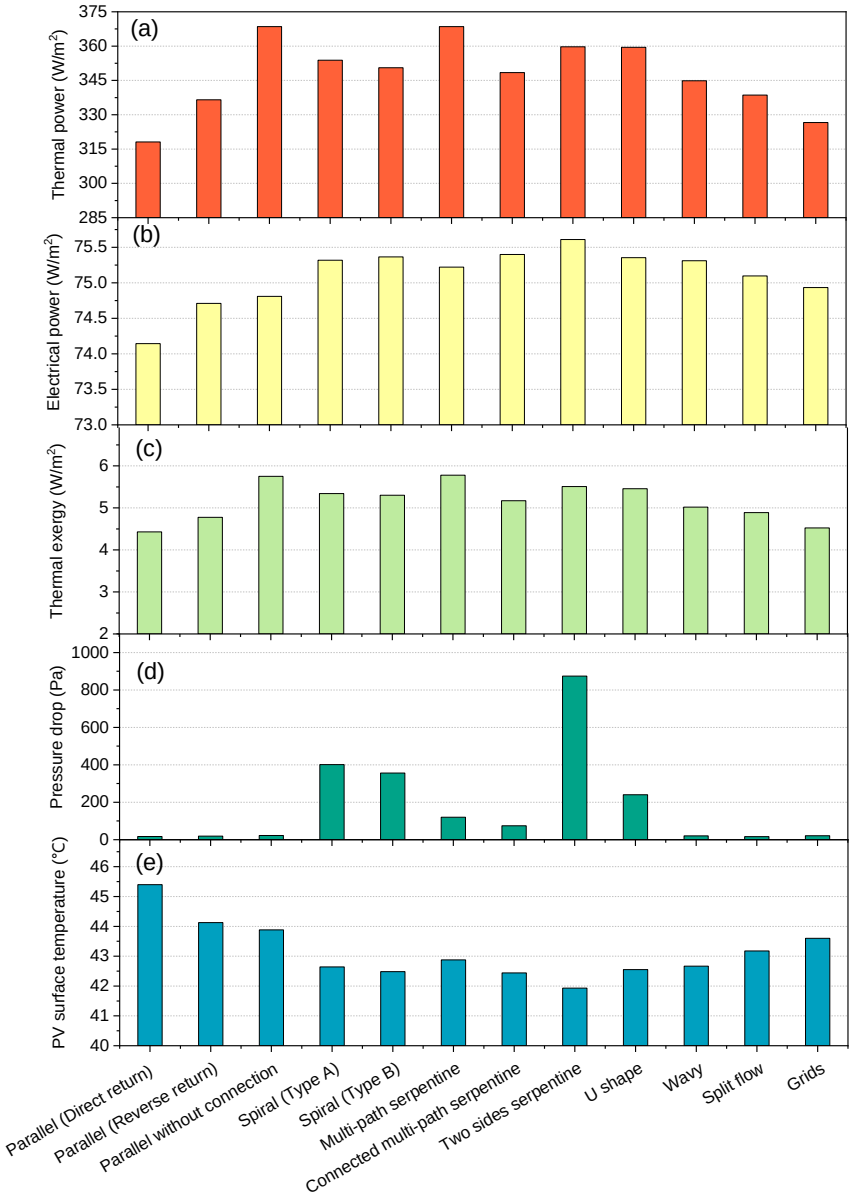

Fig 6. Comparing the effects of collector design on photovoltaic thermal systems: (a) thermal power, (b) electrical power, (c) thermal exergy, (d) pressure drop, and (e) surface temperature.

Another factor impacting the PVT output is surface temperature. When the surface temperature rises, the electrical output of the photovoltaic cells decreases due to the increased resistance. Additionally, high surface temperatures can cause solar cells to overheat, reducing their lifespan. Thus, the surface temperature of different cases is also investigated in Fig 6-(e), and the results indicate that the two-sided serpentine design with an average temperature of 41.93 °C has the

lowest temperature, while the parallel (direct return) design with the average surface temperature of 45.4 °C has the highest temperature.

To examine the system's financial viability and select the collector design with the highest possible return on investment, both the payback period and cost savings are presented in Fig 7. The design of the collector affects the amount of energy that can be collected and stored, which in turn affects the system's cost savings and payback period. The most efficient collector designs maximize the amount of energy collected and stored, leading to the lowest payback period and highest cost savings. As seen in Fig 7, the PVT system with multipath serpentine and parallel (without connection) collector designs shows the lowest payback time (2.565 and 2.567 years, respectively) and highest cost saving ($147 and $146, respectively). This is because these designs can generate the highest overall power, as shown in Fig 6. The parallel (direct return) design yields the highest payback period (2.92 years) and the lowest cost savings ($129.2) of all the designs evaluated.

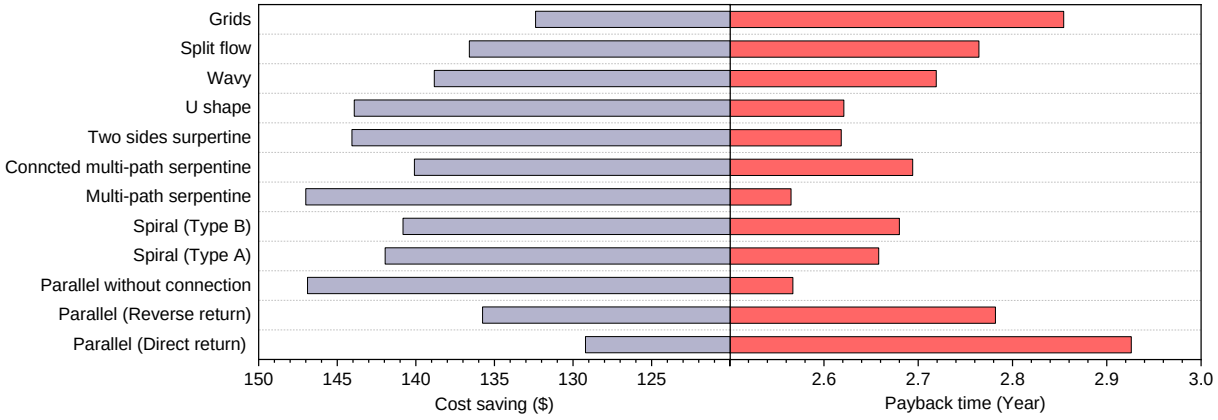

Fig 7. Comparing the payback period and cost savings of different PVT collector designs

3.2 Investigating the impact of collector and absorber materials

The material of the collector and absorber of the PVT system, which is investigated in Fig 8, is another critical factor that must be carefully chosen. The purpose of this is to ensure that the device is capable of efficiently absorbing and transferring solar energy. The absorber material should have high absorptivity and low emissivity to ensure that the maximum amount of solar radiation is absorbed. The collector tubes must also have a high thermal conductivity to achieve an efficient transfer of thermal energy to the working fluid. Thus, the PVT system output is compared with various tubes and absorbers made of various materials. Copper, aluminum, brass, and stainless steel are selected for this comparison due to their widespread availability and popularity in the market. Fig 8 demonstrates that the PVT system with copper-made collector tubes and absorber exhibits the highest electrical, thermal power, and thermal exergy. Due to its superior thermal conductivity, copper transfers heat from the absorber to the collector tubes more efficiently than aluminum. However, the weight of the PVT system with copper collector tubes and absorber was found to be 58.69 kg, making it less suitable for use in a PVT system. Aluminium, in contrast, is a better absorber of solar radiation and is more lightweight than copper, making it a better choice for use as an absorber. Nevertheless, aluminum is not as efficient as copper for conducting heat, thus making it less practical for use as a collector tube. Therefore, Case 5, with its Aluminium absorber and copper collector, is a good candidate due to its weight being 32% less than a PVT system with both its absorber and collector made of copper and its suitable high electrical and thermal power.

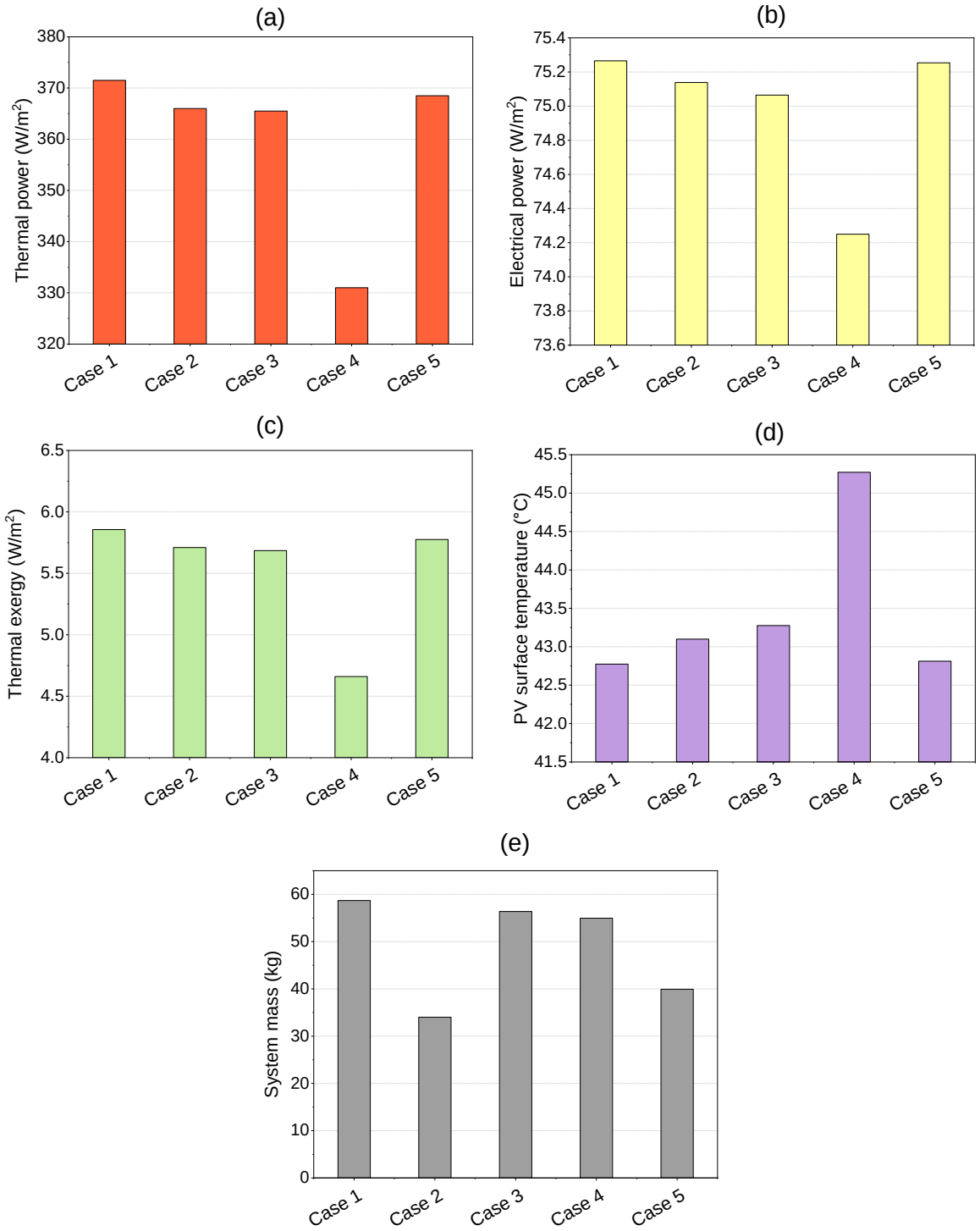

Fig 8. The effect of the material of the absorber and tubes on the PVT system performance (Case 1: absorber and collector are Copper, Case 2: absorber and collector are Aluminium, Case 3: absorber and collector are Brass, Case 4: absorber and collector are Stainless Steel, Case 5: absorber is aluminum and collector is copper)

As a result of the geometric dimensions and materials of the different units, Table 5 calculates the capital costs (see Eq.(16)). Collector's and absorber's materials have a substantial influence on payback time and annual cost savings, as demonstrated in Fig 9. Aluminium is the most cost-effective option, resulting in a payback period of 2.58 years and annual cost savings of $146.11. Assuming the system runs six months a year, the evaluation will include a PVT module with a multipath serpentine collector (Fig 2-(f)). A PVT system with an aluminum absorber and copper collector tubes is the second most cost-effective option, boasting a payback period of 3 years and annual cost savings of $146.43. Although a system with brass and stainless steel has a lower investment cost, its annual electrical and thermal power is lower than that of aluminum, resulting in a longer payback time. Copper is the most expensive option but has the highest annual electrical and thermal power. Ultimately, the selection of materials depends on the system's requirements and the available budget.

Table 4. The total cost of a PVT system with different materials for absorber and collector tubes [52] (Case 1: absorber and collector are Copper, Case 2: absorber and collector are Aluminium, Case 3: absorber and collector are Brass, Case 4: absorber and collector are Stainless Steel, Case 5: absorber is aluminum and collector is copper).

Components	Price ($)				
Materials	Case 1	Case 2	Case 3	Case 4	Case 5
PV module	200.00	200.00	200.00	200.00	200.00
Absorber	202.01	18.35	125.85	38.06	18.35
Glass	0.00	0.00	0.00	0.00	0.00
Collector pipe	63.44	5.76	39.52	11.95	63.44
Insulation	2.00	2.00	2.00	2.00	2.00
Water storage tank (120L)	34.00	34.00	34.00	34.00	34.00
Battery	55.00	55.00	55.00	55.00	55.00
Solar controller	10.00	10.00	10.00	10.00	10.00
Inverter	30.00	30.00	30.00	30.00	30.00
Total cost ($)	596.44	355.12	496.37	381.02	412.79

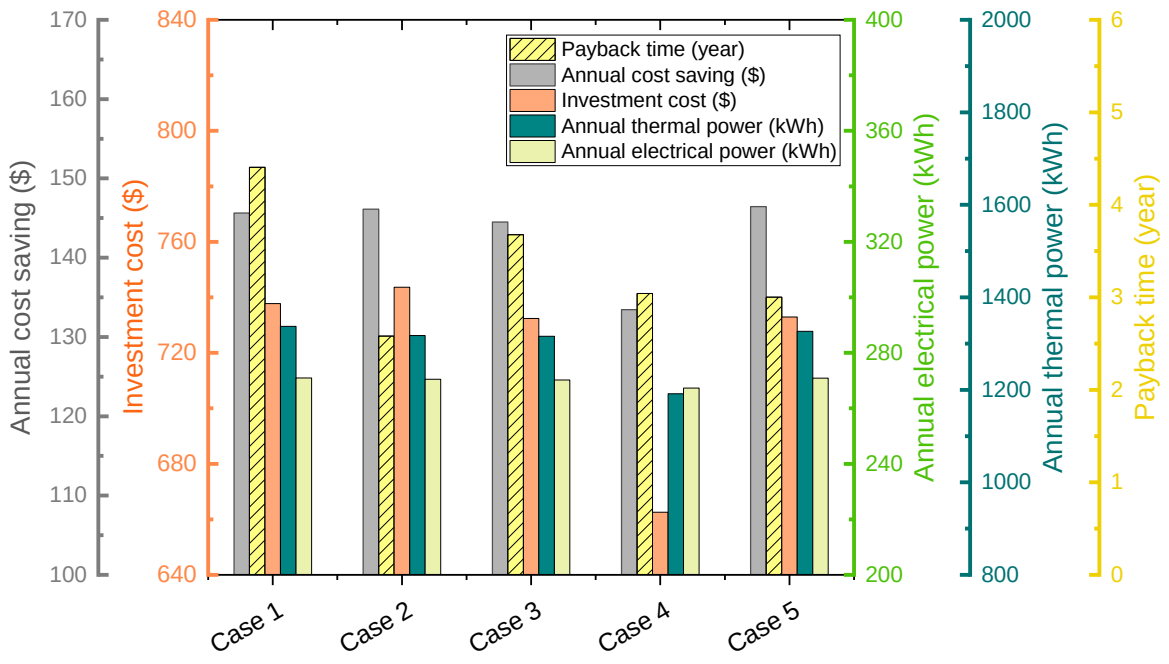

Fig 9. Comparing the impact of different collector tub and absorber materials on payback time, cost savings, investment cost, and annual thermal and electrical power output in a PVT system (Case 1: absorber and collector are Copper, Case 2: absorber and collector are Aluminium, Case 3: absorber and collector are Brass, Case 4: absorber and collector are Stainless Steel, Case 5: absorber is aluminum and collector is copper).

3.3 Investigating the effect of collector length

Fig 10 illustrates the influence of collector length in photovoltaic thermal systems, which is crucial in determining the amount of energy that can be harvested and converted into usable heat. To determine the optimal length of the thermal management layers, a detailed calculations is performed in this section and evaluats various collector lengths to determine their effects on system energy and exergy output, pressure drop, weight, and cost. It should be noted that the PVT system with multipath serpentine collector design (Fig 2-(f)) is considered for this evaluation.

This figure shows that a longer collector length allows the system to capture more solar energy, resulting in lower surface temperatures and more power. The results indicated that electrical power, thermal power, and thermal exergy improved on average by 0.59%, 2.81%, and 3.84%, respectively when the length increased from 14.7 to 29 m. In addition, the pressure drop increases if the collector is longer. This is due to the increased surface area and bends in the longer collector, creating more fluid flow resistance. The pressure drop is enhanced by 116.34 Pa when the collector is increased from 14.7 to 29 m.

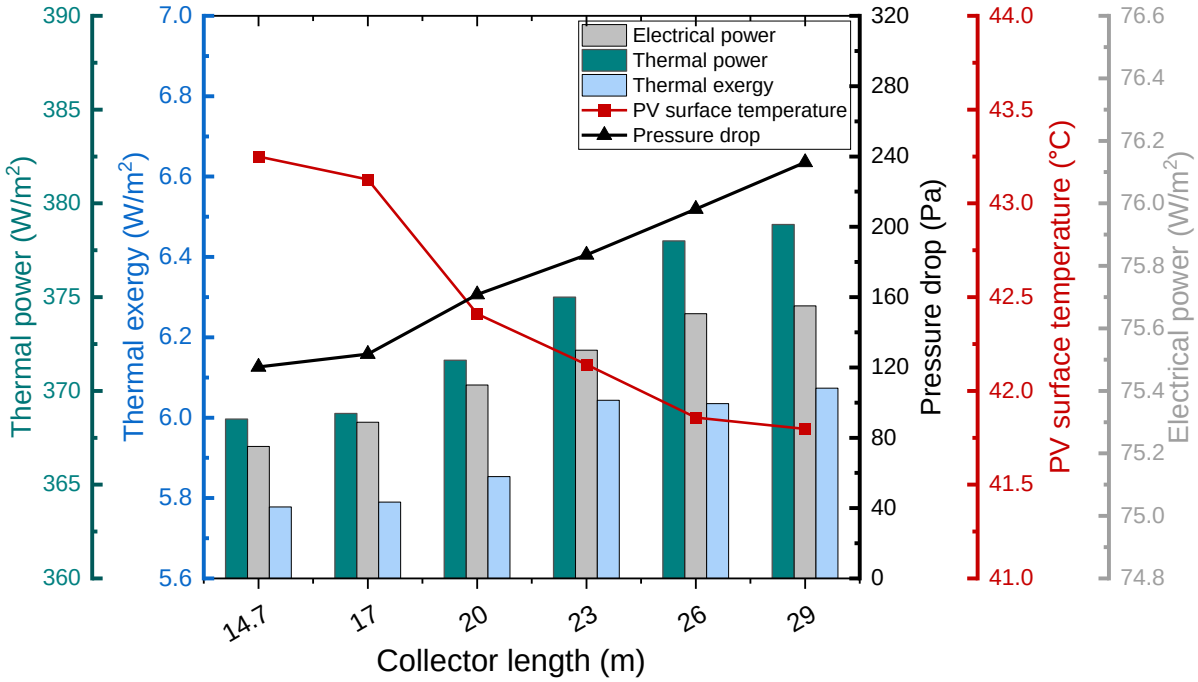

Fig 10. Evaluating the contribution of collector length on energy, exergy, surface temperature, and pressure drop in photovoltaic thermal systems

Fig 11 presents an economic evaluation of the output of the PVT system with varying collector lengths. The PVT system with multipath serpentine collector design (Fig 2-(f)) with aluminum absorber and collector tube is considered for this evaluation. As seen in Fig 11-(a), longer collectors increase the annual thermal and electrical powers because the system with longer collectors is able

to capture more energy from the sun, resulting in higher efficiency. Additionally, longer collectors can reduce the amount of energy lost through heat transfer, further increasing the system's efficiency and resulting in greater cost savings. Thus, the collector length enhancement from 14.7 to 29 m has improved the cost by saving 2.5% (see Fig 11-(b)). Based on Fig 11-(b), the collector length of a PVT system directly impacts its payback time.

Table 5. The total cost of a PVT system with varying collector lengths [52].

Components	Price ($)					
Collector length (m)	14.7	16	20	23	26	29
PV module	200.00	200.00	200.00	200.00	200.00	200.00
Absorber (Aluminium)	18.35	18.35	18.35	18.35	18.35	18.35
Glass	0.00	0.00	0.00	0.00	0.00	0.00
Collector pipe (Aluminium)	5.76	6.27	7.83	9.01	10.18	11.36
Insulation	2.00	2.00	2.00	2.00	2.00	2.00
Water storage tank (120L)	34.00	34.00	34.00	34.00	34.00	34.00
Battery	55.00	55.00	55.00	55.00	55.00	55.00
Solar controller	10.00	10.00	10.00	10.00	10.00	10.00
Inverter	30.00	30.00	30.00	30.00	30.00	30.00
Total cost ($)	355.12	355.62	357.19	358.36	359.53	360.71

The longer the collector length, the more energy can be collected and converted into usable electricity and heat. Thus, the system could generate more electricity in less time, resulting in a shorter payback time. However, the total cost (Table 5) and weight of PVT systems can be negatively impacted by a long collector length. A longer collector length requires more material, raising the system's price. Additionally, the longer the collector length, the heavier the system will be, which can make it more difficult to install and transport, as seen in Fig 11-(d). Therefore, selecting the collector length for a PVT system requires balancing cost, weight, and performance.

It is worth clarifying that the collector tube and the absorber plate are two separate components of the PVT system, as shown in Fig 2. The collector tube is represented by the purple color, while the absorber plate is represented by the yellow color. In this section, only the length of the collector tube is changed, and the length of the absorber plate remains constant. Therefore, the cost of the absorber plate remains constant regardless of the length of the collector tube, as shown in Table 5.

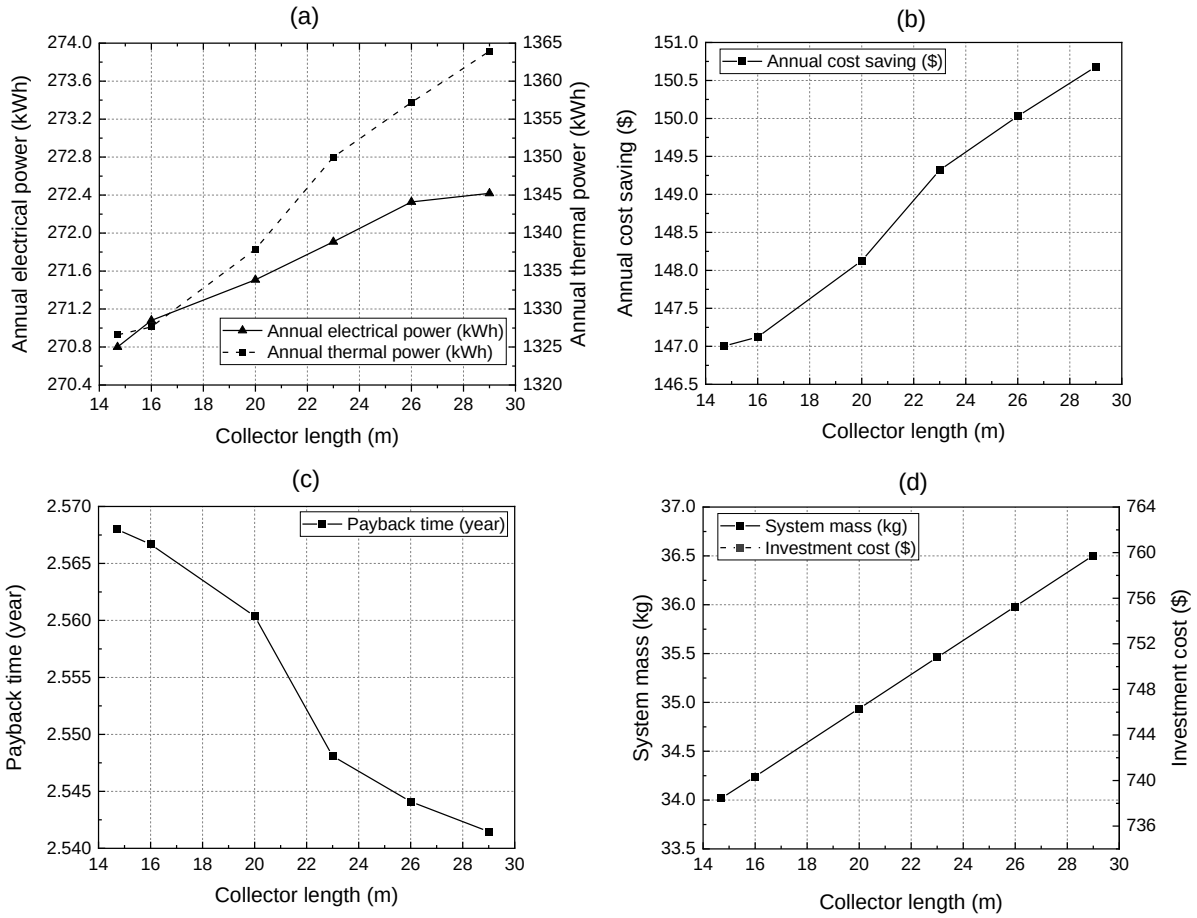

Fig 11. Comparing the impact of different collector lengths on payback time, cost savings, investment cost, and annual thermal and electrical power output in a PVT system

4 Conclusions

This study investigated various collector configurations to provide the effective one with respect to electrical and thermal power, exergy, and pressure drop. The configurations considered included

parallel, spiral, serpentine, wavy, grid, multipath design and split flow. Additionally, various materials were considered for the collector tubes and absorbers, such as copper, aluminum, brass, and stainless steel. High generated powers, low price, and light weight were desired goals for selecting a suitable material. Moreover, the total length of the collector tubes was evaluated for its effect on energy and exergy performances, cost, payback period, and total weight. This study has yielded the following findings:

- The surface temperature is highest in the parallel (direct return) collector design, and the two-sided serpentine design has the lowest surface temperature.
- The multipath serpentine design is the most effective in terms of overall power, with an average overall power output of 443.71 W/m^2. In comparison, the parallel (direct return) collector design has the lowest overall power output of 392.26 W/m^2.
- Two-sided serpentine collectors have higher pressure drops (874 Pa), while designs with smoother tube paths, such as parallel tubes, split flow, and wavy, have lower pressure drops (less than 22 Pa).
- PVT system with aluminum is the most cost-effective option, with a payback time of 2.58 years and annual cost savings of $146.11. Moreover, the system's total weight with aluminum is 42% lighter than the system with copper.
- The electrical power, thermal power, and thermal exergy improved on average by 0.59%, 2.81%, and 3.84%, respectively, when the length increased from 14.7 to 29 m.

Overall, the selection of the best collector design for photovoltaic thermal systems depends on the application and the customer's desire. Different designs have different advantages and disadvantages. For example, some designs have high overall power output, but their pressure drop, weight, and surface temperature are also high. On the other hand, some designs have low-pressure

drop, lightweight, and low surface temperature, but their overall power output is lower. Therefore, it is important to consider the application and customer's desire when selecting the best collector design for photovoltaic thermal systems.

5 Acknowledgments

This work was supported by the finical support from National Key R&D Program of China through Grant 2022YFB4200902 and the Joint Postdoctoral Scheme with Non-local Institutions of The Hong Kong Polytechnic University.

6 References

[1] Pathak SK, Sharma PO, Goel V, Bhattacharyya S, Aybar HŞ, Meyer JP. A detailed review on the performance of photovoltaic/thermal system using various cooling methods. Sustainable Energy Technologies and Assessments. 2022;51:101844.
[2] Maadi SR, Khatibi M, Ebrahimnia-Bajestan E, Wood D. Coupled thermal-optical numerical modeling of PV/T module – Combining CFD approach and two-band radiation DO model. 2019;198.
[3] Hossain M, Kumar L, Nahar A. A Comparative Performance Analysis between Serpentine-Flow Solar Water Heater and Photovoltaic Thermal Collector under Malaysian Climate Conditions. International Journal of Photoenergy. 2021;2021:1-9.
[4] He W, Yi JS, Van Nguyen T. Two-phase flow model of the cathode of PEM fuel cells using interdigitated flow fields. AIChE Journal. 2000;46:2053-64.
[5] Ghanbarian A, Kermani MJ, Scholta J, Abdollahzadeh M. Polymer electrolyte membrane fuel cell flow field design criteria–application to parallel serpentine flow patterns. Energy conversion and management. 2018;166:281-96.
[6] El-Zoheiry RM, Mori S, Ahmed M. Using multi-path spiral flow fields to enhance under-rib mass transport in direct methanol fuel cells. International Journal of Hydrogen Energy. 2019;44:30663-81.
[7] Poredoš P, Tomc U, Petelin N, Vidrih B, Flisar U, Kitanovski A. Numerical and experimental investigation of the energy and exergy performance of solar thermal, photovoltaic and photovoltaic-thermal modules based on roll-bond heat exchangers. Energy conversion and management. 2020;210:112674.
[8] Fudholi A, Sopian K, Yazdi MH, Ruslan MH, Ibrahim A, Kazem HA. Performance analysis of photovoltaic thermal (PVT) water collectors. Energy conversion and management. 2014;78:641-51.
[9] Palaskar V, Deshmukh S. A critical review on enhancement in system performance of flat plate hybrid PV/T solar collector system. International Journal of Energy Science. 2013;3:395-402.

[10] Hossain M, Pandey A, Selvaraj J, Abd Rahim N, Islam M, Tyagi V. Two side serpentine flow based photovoltaic-thermal-phase change materials (PVT-PCM) system: Energy, exergy and economic analysis. Renewable Energy. 2019;136:1320-36.
[11] Eisapour AH, Eisapour M, Hosseini M, Shafaghat A, Sardari PT, Ranjbar A. Toward a highly efficient photovoltaic thermal module: Energy and exergy analysis. Renewable Energy. 2021;169:1351-72.
[12] Shahsavar A. Experimental evaluation of energy and exergy performance of a nanofluid-based photovoltaic/thermal system equipped with a sheet-and-sinusoidal serpentine tube collector. Journal of Cleaner Production. 2021;287:125064.
[13] Hosseinzadeh M, Salari A, Sardarabadi M, Passandideh-Fard M. Optimization and parametric analysis of a nanofluid based photovoltaic thermal system: 3D numerical model with experimental validation. Energy Conversion and Management. 2018;160:93-108.
[14] Maadi SR, Navegi A, Solomin E, Ahn HS, Wongwises S, Mahian O. Performance improvement of a photovoltaic-thermal system using a wavy-strip insert with and without nanofluid. Energy. 2021;234:121190.
[15] Maadi SR, Khatibi M, Ebrahimnia-Bajestan E, Wood D. Coupled thermal-optical numerical modeling of PV/T module–Combining CFD approach and two-band radiation DO model. Energy conversion and management. 2019;198:111781.
[16] Jia Y, Ran F, Zhu C, Fang G. Numerical analysis of photovoltaic-thermal collector using nanofluid as a coolant. Solar Energy. 2020;196:625-36.
[17] Shahsavar A, Eisapour M, Talebizadehsardari P. Experimental evaluation of novel photovoltaic/thermal systems using serpentine cooling tubes with different cross-sections of circular, triangular and rectangular. Energy. 2020;208:118409.
[18] Huang X, Li F, Xiao T, Guo J, Wang F, Gao X, et al. Investigation and optimization of solidification performance of a triplex-tube latent heat thermal energy storage system by rotational mechanism. Applied Energy. 2023;331:120435.
[19] Du Z, Liu G, Huang X, Xiao T, Yang X, He Y-L. Numerical studies on a fin-foam composite structure towards improving melting phase change. International Journal of Heat and Mass Transfer. 2023;208:124076.
[20] Li F, Huang X, Li Y, Lu L, Meng X, Yang X, et al. Application and analysis of flip mechanism in the melting process of a triplex-tube latent heat energy storage unit. Energy Reports. 2023;9:3989-4004.
[21] Cameron WJ, Reddy KS, Mallick TK. Review of high concentration photovoltaic thermal hybrid systems for highly efficient energy cogeneration. Renewable and Sustainable Energy Reviews. 2022;163:112512.
[22] Umam MF, Hasanuzzaman M, Rahim NA. Global Advancement of Nanofluid-Based Sheet and Tube Collectors for a Photovoltaic Thermal System. Energies. 2022;15:5667.
[23] Wilberforce T, El Hassan Z, Ogungbemi E, Ijaodola O, Khatib F, Durrant A, et al. A comprehensive study of the effect of bipolar plate (BP) geometry design on the performance of proton exchange membrane (PEM) fuel cells. Renewable and sustainable energy reviews. 2019;111:236-60.
[24] Yu Q, Romagnoli A, Yang R, Xie D, Liu C, Ding Y, et al. Numerical study on energy and exergy performances of a microencapsulated phase change material slurry based photovoltaic/thermal module. Energy conversion and management. 2019;183:708-20.
[25] Pierrick H, Christophe M, Leon G, Patrick D. Dynamic numerical model of a high efficiency PV–T collector integrated into a domestic hot water system. Solar Energy. 2015;111:68-81.

[26] Michael JJ, Selvarasan I, Goic R. Fabrication, experimental study and testing of a novel photovoltaic module for photovoltaic thermal applications. Renewable Energy. 2016;90:95-104.
[27] Patankar S. Numerical heat transfer and fluid flow: CRC press; 1980.
[28] Bovand M, Rashidi S, Dehghan M, Esfahani J, Valipour M. Control of wake and vortex shedding behind a porous circular obstacle by exerting an external magnetic field. Journal of Magnetism and Magnetic Materials. 2015;385:198-206.
[29] Rashidi S, Esfahani J. The effect of magnetic field on instabilities of heat transfer from an obstacle in a channel. Journal of Magnetism and Magnetic Materials. 2015;391:5-11.
[30] Herrando M, Ramos A, Zabalza I, Markides CN. A comprehensive assessment of alternative absorber-exchanger designs for hybrid PVT-water collectors. Applied energy. 2019;235:1583-602.
[31] Maadi SR, Sabzali H, Kolahan A, Wood D. Improving the performance of PV/T systems by using conical-leaf inserts in the coolant tubes. Solar Energy. 2020;212:84-100.
[32] Preet S, Bhushan B, Mahajan T. Experimental investigation of water based photovoltaic/thermal (PV/T) system with and without phase change material (PCM). Solar Energy. 2017;155:1104-20.
[33] Joshi AS, Tiwari A. Energy and exergy efficiencies of a hybrid photovoltaic–thermal (PV/T) air collector. Renewable Energy. 2007;32:2223-41.
[34] Kazemian A, Salari A, Ma T, Lu H. Application of hybrid nanofluids in a novel combined photovoltaic/thermal and solar collector system. Solar Energy. 2022;239:102-16.
[35] Kazemian A, Parcheforosh A, Salari A, Ma T. Optimization of a novel photovoltaic thermal module in series with a solar collector using Taguchi based grey relational analysis. Solar Energy. 2021;215:492-507.
[36] Salari A, Kazemian A, Ma T, Hakkaki-Fard A, Peng J. Nanofluid based photovoltaic thermal systems integrated with phase change materials: Numerical simulation and thermodynamic analysis. Energy Conversion and Management. 2020;205:112384.
[37] Kazemian A, Khatibi M, Ma T, Peng J, Hongxing Y. A thermal performance-enhancing strategy of photovoltaic thermal systems by applying surface area partially covered by solar cells. Applied Energy. 2023;329:120209.
[38] Kazemian A, Salari A, Hakkaki-Fard A, Ma T. Numerical investigation and parametric analysis of a photovoltaic thermal system integrated with phase change material. Applied energy. 2019;238:734-46.
[39] Swinbank WC. Long-wave radiation from clear skies. Quarterly Journal of the Royal Meteorological Society. 1963;89:339-48.
[40] Maadi SR, Khatibi M, Ebrahimnia-Bajestan E, Wood D. A parametric study of a novel PV/T system model which includes the greenhouse effect. 2019.
[41] Chow TT, Pei G, Fong K, Lin Z, Chan A, Ji J. Energy and exergy analysis of photovoltaic–thermal collector with and without glass cover. Applied Energy. 2009;86:310-6.
[42] Park SR, Pandey AK, Tyagi VV, Tyagi SK. Energy and exergy analysis of typical renewable energy systems. Renewable and Sustainable Energy Reviews. 2014;30:105-23.
[43] Said Z, Saidur R, Rahim NA, Alim MA. Analyses of exergy efficiency and pumping power for a conventional flat plate solar collector using SWCNTs based nanofluid. Energy and Buildings. 2014;78:1-9.
[44] Kazemian A, Taheri A, Sardarabadi A, Ma T, Passandideh-Fard M, Peng J. Energy, exergy and environmental analysis of glazed and unglazed PVT system integrated with phase change material: An experimental approach. Solar Energy. 2020;201:178-89.

[45] Herrando M, Pantaleo AM, Wang K, Markides CN. Solar combined cooling, heating and power systems based on hybrid PVT, PV or solar-thermal collectors for building applications. Renewable Energy. 2019;143:637-47.
[46] IEA N. Projected costs of generating electricity. International Energy Agency. 2010;10:618.
[47] https://www.globalpetrolprices.com/China.
[48] Hartmann N, Glueck C, Schmidt F. Solar cooling for small office buildings: Comparison of solar thermal and photovoltaic options for two different European climates. Renewable Energy. 2011;36:1329-38.
[49] Khanjari Y, Kasaeian A, Pourfayaz F. Evaluating the environmental parameters affecting the performance of photovoltaic thermal system using nanofluid. Applied Thermal Engineering. 2017;115:178-87.
[50] Selmi M, Al-Khawaja MJ, Marafia A. Validation of CFD simulation for flat plate solar energy collector. Renewable energy. 2008;33:383-7.
[51] Salari A, Hakkaki-Fard A. A numerical study of dust deposition effects on photovoltaic modules and photovoltaic-thermal systems. Renewable Energy. 2019;135:437-49.
[52] https://www.alibaba.com.